A Hybrid Knee Exoskeleton Using Real-Time Ultrasound-Based Muscle Fatigue Assessment

Zhiyu Sheng, Ashwin Iyer, Ziyue Sun, Kang Kim, Nitin Sharma

***Abstract*—Ultrasound-based state assessment of the human muscle during rehabilitation and its integration into a hybrid exoskeleton comprising an functional electrical stimulation (FES) system and a powered orthosis are emerging research areas. This paper presents results from the first experimental demonstration of a hybrid knee exoskeleton that uses ultrasound-derived muscle state feedback to coordinate electrical motors and FES. A significant contribution of the paper is to integrate a real-time ultrasound image acquisition and processing framework into a recently derived switching-based feedback control of the hybrid knee exoskeleton. As a result, the contractility response of the quadriceps muscle to the FES input can be monitored in vivo in real-time and estimate FES-induced muscle fatigue changes in the muscle. The switched controller's decision-making process can then use the estimated muscle fatigue to compensate or replace the FES-stimulated muscle power with an electrical motor, thus avoiding extensive stimulation of the fatigued muscle. The experimental results suggest a potential application in the rehabilitation of neurological disorders like spinal cord injuries and stroke.**

I. Introduction

Functional electrical stimulation (FES) is a rehabilitative technique that may assist impaired motor functions such as hand grasping, trunk movement, and gait in individuals with a neurological injury such as spinal cord injury, stroke, multiple sclerosis, etc. [1]–[10]. Despite its significant potential, the rapid onset of FES-induced muscle fatigue hinders its use in clinics and in activities of daily living. Recently, the addition of a powered orthosis to FES improved its control performance despite FES-caused adverse fatigue effects [11]–[18]. Arguably, the powered orthosis can also be used for assistance solely [19], [20] and may have a competitive edge over FES due to its unrestrained and robust power generation. However, replacing FES with powered orthosis may prove disadvantageous because incorporating FES exercises the muscle and brings many potential training/therapeutic effects [21] [22], [23]. Therefore, a combined FES system and a powered exoskeleton is a promising rehabilitation system for individuals with mobility disorders. However, the design and control of a hybrid exoskeleton being a new and emerging research area, numerous challenges in their design and control hinder their clinical implementation.

First, the hybrid exoskeleton must compensate for the declining muscle force due to that rapid onset of FES-induced muscle fatigue. The muscle fatigue results from non-physiological recruitment of muscle motor units, i.e., recruitment is asynchronous and spatially fixed [24]. The fatigued muscle cannot maintain the same muscle power output to actuate the limb joints. Thus, the muscle output cannot maintain desired limb tracking, constraining functional tasks to short periods. Therefore, a specifically designed control strategy must maintain a long operation given the decreasing contribution of FES-recruited muscle power. The hybrid exoskeleton control scheme may use cooperation or a switched strategy to allocate control inputs among external actuators and FES.

Further, it should be capable of completely replacing the FES-elicited muscle power with the powered orthosis when the muscle potentially experiences an acute fatigue condition while guaranteeing the system stability. Recent control algorithms for a hybrid exoskeleton facilitate cooperative use of FES and the exoskeleton [11]–[14]. However, a control approach that automates exoskeleton assistance during acute FES-caused muscle failure due to the fatigue and turns-on the FES use when the muscle recovers from the fatigue is lacking. Our recent work proposed a generic theoretical framework [25] for FES-elicited muscles in closed-loop with a wearable robotic system that considers the FES-evoked muscle's fatigue and recovery cycle. The designed switch criteria coordinate FES-elicited muscle power and external actuators while ensuring the hybrid exoskeleton's stability despite nonlinearity, uncertainty, and electromechanical delay (EMD) in the musculoskeletal system.

Another challenge is that the lack of sensors to measure muscle fatigue during FES limits effective control of the hybrid exoskeleton. Advanced switched control techniques for hybrid exoskeleton monitor different switch criteria [25] among multiple actuators to ensure system stability and control performance. The switching criteria need measures or estimates of the system state that include the joint angle, joint velocity, and FES-induced changes in muscle condition. Predictive mathematical models [26]–[30] have been used to estimate changes in muscle condition. Compared to those model-only approaches, we believe that introducing real-time direct measurements can better assist controller's decision

Manuscript submitted January 20, 2022, revised April 1, 2022, accepted April 20, 2022. This work is supported by NSF award number: 1646009. Any opinions, findings and conclusions or recommendations expressed in this material are those of the authors and do not necessarily reflect the views of NSF. *(Corresponding authors: Kang Kim and Nitin Sharma)*

Zhiyu Sheng and Kang Kim are with the Department of Medicine, University of Pittsburgh School of Medicine and University of Pittsburgh Medical Center, Pittsburgh, PA, USA. e-mail: zhs41@pitt.edu, kangkim@upmc.edu. Ashwin Iyer, Ziyue Sun and Nitin Sharma are with the Joint Department of Biomedical Engineering, North Carolina State University, Raleigh, NC, USA. email: aiyer3@ncsu.edu, zsun32@ncsu.edu, nsharm23@ncsu.edu. Kang Kim are also with the Department of Bioengineering and the Department of Mechanical Engineering and Materials Science, University of Pittsburgh School of Engineering, Pittsburgh, PA, USA. Kang Kim is also with the McGowan Institute for Regenerative Medicine, University of Pittsburgh and University of Pittsburgh Medical Center, Pittsburgh, PA, USA.

making because the direct measurements provide feedback of the most updated muscle condition, which can then mitigate the estimate errors (due to signal processing noise and modeling uncertainties) accumulated over time. However, the direct and real-time measurement of the muscle condition due to the induced fatigue is infeasible with the typically used sensors in robotic devices (e.g., encoder, strain gauge, inertia measurement units, etc.). To address this challenge, we sought a new sensing modality to characterize and monitor FES-induced muscle contractility changes in vivo.

Ultrasound has been an essential and valuable tool in clinical diagnosis, rehabilitation, and research investigation of human skeletal muscle [31]–[39]. Researchers have recently started developing ultrasound image processing algorithms that enable real-time ultrasound imaging into robotics and prosthetic devices for human augmentation and rehabilitation. Castellini et al. [40] and González et al. [41] proposed an ultrasound-based human-machine interface that predicts finger positions and forces from processed ultrasound images. Sikdar et al. [42] developed a wearable ultrasonic system that can classify and predict dexterous individual finger movements. In our previous studies [43], [44], we used ultrasound speckle tracking algorithm [45] for tissue motion estimation. The estimated muscle displacement was then used to compute the strain tensor to capture the quadriceps muscle contractility change that was hypothesized as an effect of FES-induced fatigue. The approach was validated on several human participants and demonstrated that the ultrasound-based technique can estimate FES-induced muscle fatigue.

Compared to other sensor modalities such as dynamometers, surface electromyography (sEMG), and mechanomyogram (MMG), ultrasound imaging provides both anatomical and functional information, and thus a potential sensing solution for effective hybrid exoskeleton control. Ultrasound imaging is relatively low cost and facilitates a real-time setup, compared to other clinical imaging modalities like magnetic resonance imaging (MRI). In addition, recent advancements in portable ultrasound devices [46]–[48] promise its integration in a compact wearable robotic system. However, to enable ultrasound-based feedback control, the capability of real-time data acquisition is critical because the controller relies on the acquired and most updated information to make control decisions. The real-time characteristic of ultrasound imaging noted in the literature mainly refers to the image acquisition and reconstruction without further image processing for tissue motion estimation. However, the tissue motion estimation is vital to derive muscle contractility-related changes for fatigue estimation. Implementation of this process is a non-trivial problem. It entails accelerating the computation of a tremendous amount of image data to perform the ultrasound speckle tracking algorithm, the primary computation-consuming part.

Nevertheless, a graphic processor unit (GPU) offers a potential resource to accelerate the computation. Primarily, the core structure of the speckle tracking algorithm is a kernel-based similarity matching, which allows simultaneous parallel computation at different independent local image coordinates. As a result, conceptually, the processing time is unlikely to increase when the data size grows apparently. Several works in the literature [49], [50] have implemented this idea in different GPU-based platforms. In our current study, considering the requirement of up-sampling the images to capture small local displacements, the available memory size of the current generation of GPUs is another limitation. Therefore, we tried finding a trade-off between the total computation time and the image quality to overcome this challenge. We implemented our algorithm in a semi-parallel structure, dividing every single image into several pieces of sub-image and loading them on the GPU consecutively. The parallel computation was then performed on each loaded sub-images, and the processed results were assembled at the end.

After achieving the real-time ultrasound speckle tracking algorithm, the imaging processing procedure can be deployed in feedback control of a hybrid exoskeleton to estimate muscle's fatigue state and assist the controller's decision-making. As a result, in this paper, we first model and design a 1-degree-of-freedom (1-DOF) hybrid knee exoskeleton that collaboratively uses an electrical motor at the knee joint and applies FES to the quadriceps-hamstring muscle group. We then implement a newly derived switched control method. The control objective uses different control modes to track desired knee joint movements. The first mode collaboratively uses FES-activated muscle power and an electrical motor, while the second mode only uses all electrical motor power. The two modes are switched and are active in turns, subject to switch criteria determined by the stability constraints and the muscle fatigue state. The control design is robust to modeling uncertainties and compensates for the EMD. We finally integrated the hybrid knee exoskeleton with the developed real-time ultrasound image acquisition and processing platform. To the best of our knowledge, the presented results for the first time experimentally demonstrate real-time measurement of the muscle state due to the induced muscle fatigue via ultrasound-derived strain measures and its integration into feedback for the hybrid exoskeleton controller's decision-making.

II. Methods

A. Modeling and Switched Control Design of the 1-DOF Hybrid Knee Exoskeleton

A generalized theoretical framework for an N-degree of freedom wearable robot was proposed in [25]. Here we adapt the framework for a 1-DOF hybrid knee exoskeleton that can be modeled as

$$J\ddot{q} + Mgl_{COM}\sin(q + q_0) + M_{ev}(q, \dot{q}) + W = \tau_t \quad (1)$$

where, $q \in \mathbb{R}$ denotes the knee joint angle as illustrated in Fig. 1. The constant, $q_0 \in \mathbb{R}$, is an initial offset angle with respect to the vertical direction. The constant, $J \in \mathbb{R}_{>0}$, denotes the moment of inertia of the lower leg with respect to the fixed axis, which the knee joint rotates around. The constants, $M \in \mathbb{R}_{>0}$, $l_{COM} \in \mathbb{R}_{>0}$ are the mass of the lower leg and the distance between the knee joint and the center of mass (COM) of the lower leg, respectively. $M_{ev}(q, \dot{q}) \in \mathbb{R}$ expresses a bounded unknown passive moment due to the elastic-viscous effect at the knee joint, as well as the viscous friction of the exoskeleton assembly. $W \in \mathbb{R}$ represents a

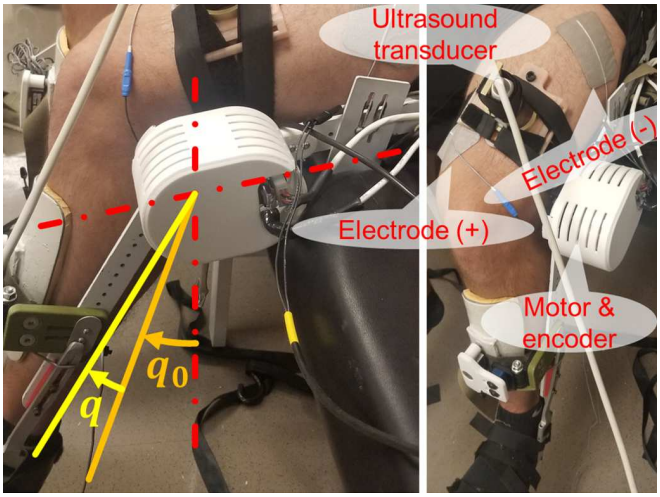

Figure 1. Experimental setup of the 1-DOF hybrid knee exoskeleton experiments. The dashed-dotted red lines illustrate the horizontal and vertical directions. q_0, as illustrated by the solid orange line, is the initial offset angle and is approximately 45°. The encoder registered knee joint angle, q, as illustrated by the solid yellow line. It is defined as the angle with respect to q_0. The knee joint is actuated by the electrical motor, which contains an internal encoder, and also on the application of FES to the quadriceps muscle. A pair of large electrode pads placed on the thigh and the other pair to stimulate the hamstring (cannot be seen in the presented photo) apply electrical current to the muscles. A clinical ultrasound imaging transducer is attached to the thigh in a longitudinal direction, where the lateral direction of the ultrasound image aligns with the direction of muscle fibers, by using a lab-built probe holder.

bounded unknown disturbance term and $\tau_t \in \mathbb{R}$ is the total torque input to the system from both FES and motors. The total torque can be further specified as

$$\begin{aligned}\tau_t = &\frac{1+\xi_{\tau^{(1)}}}{2}\hat{\mu}^{(1)}\eta^{(1)}K_a^{(1)}u_{s,\tau^{(1)}}^{(1)} \\ &- \frac{1+\xi_{\tau^{(2)}}}{2}\hat{\mu}^{(2)}\eta^{(2)}K_a^{(2)}u_{s,\tau^{(2)}}^{(2)} \\ &+ \frac{1+\xi}{2}K_m u_{m_I} + \frac{1-\xi}{2}K_m u_{m_{II}},\end{aligned} \tag{2}$$

where $K_m \in \mathbb{R}_{>0}$ is the motor constant while $u_{m_I}(t) \in \mathbb{R}$ and $u_{m_{II}}(t) \in \mathbb{R}$ are control inputs to the electric motors under control mode I and II, respectively.

Control mode I uses a PD-based delay compensation controller to facilitate the existence of EMDs when both FES and the electrical motor are active to drive the knee joint. Control mode II uses a variable structure control (VSC) when only the electrical motor is active. $\eta^{(j)}(q,\dot{q}) \in \mathbb{R}_{>0}$ is a lumped bounded unknown nonlinear function that maps a positive input delayed FES control signal (current, in mA), $u_{a,\tau^{(j)}}^{(j)} = u_a^{(j)}(t-\tau^{(j)}) \in \mathbb{R}_{>0}$, where $t \in \mathbb{R}$ is the time and the superscript $j = 1$ refers to the quadriceps muscle while $j = 2$ refers to the hamstring muscle. $\tau^{(j)} \in \mathbb{R}_{>0}$ are the corresponding EMDs associated with the two muscle groups. $K_a^{(j)} \in \mathbb{R}_{>0}$ is a control gain to modulate $u_s^{(j)}$. $\xi(t) \in \{-1, 1\}$ is a switch signal. $\xi = 1$ indicates control mode I and $\xi = -1$ indicates control mode II. $\xi_{\tau^{(j)}}$, $j = 1, 2$ is the delayed signal similar to the definition of $u_{a,\tau^{(j)}}^{(j)}$. The value of the switch signal is determined by $\hat{\mu}^{(j)}(t) \in [\varsigma^{(j)}, 1]$, which is the estimate of the FES-induced muscle fatigue, where $\varsigma^{(j)} \in \mathbb{R}$ is the lower bound of $\hat{\mu}^{(j)}$.

B. Feedback Controller for Switched Modes

The feedback control law that determines the FES inputs to the quadriceps and hamstrings of the system in (1) and (2), is given by

$$\begin{aligned}u_s^{(1)} &= K_u \tfrac{1+\text{sgn}(r)}{2}\rho_s \text{sgn}(r)\, r \\ u_s^{(2)} &= K_u \tfrac{1-\text{sgn}(r)}{2}\rho_s \text{sgn}(r)\, r,\end{aligned} \tag{3}$$

the motor input in mode I is

$$u_{m_{\text{I}}} = K_u \rho_m r, \tag{4}$$

and the motor input in mode II is

$$u_{m_{II}} = \frac{1}{K_m}\left(\frac{r}{|r|+r_c}\left(\delta\Phi'(\left\|(e,r)^T\right\|)\left\|(e,r)^T\right\| + \Psi'\right) + K_v r\right), \tag{5}$$

where, the control error signal, $r(t) \in \mathbb{R}$, is defined as

$$r = \dot{e} + \alpha e - \frac{\xi+1}{2}\beta e_c. \tag{6}$$

where, $e = q_d - q \in \mathbb{R}$ is the tracking error between the actual and desired knee joint angle, q and q_d, respectively. $e_c = \int_{t-\tau^{(1)}}^{t} u_s^{(1)}(\theta)d\theta - \int_{t-\tau^{(2)}}^{t} u_s^{(2)}(\theta)d\theta \in \mathbb{R}$ is a delay compensation term. K_u, ρ_s, ρ_m, r_c, K_v, α and β are control gains. $\delta\Phi'(\left\|(e,r)^T\right\|)$ is a positive globally invertible non-decreasing function of the norm of the tracking error signal, and is appropriately selected to bound the state dependent uncertainties. Ψ' is a constant used to bound all the other disturbance or uncertainties. The choice and tuning of all these control gains and parameters follow Theorem 1 and Theorem 2 in [25]. The switch signal, ξ, follows almost the same switch criteria as given by Theorem 3 in [25]. The only two modifications are that: 1) In this paper, we only consider the knee joint and the muscle fatigue of the quadriceps muscle in the implementation of this very first experiment; 2) In experiments of this paper, the stability constraints in the general switch criteria (as given by [25]) would be trivially satisfied in practice because the fatigue/recovery time constants are much longer compared to the convergence time of the designed control mode $u_{m_{\text{I}}}$ and $u_{m_{\text{II}}}$. The switch criteria is therefore dominated by the estimated fatigue state. As a result, control $u_{m_{\text{I}}}$ is active to use both electrical motors and FES when muscle is non-fatigued while control $u_{m_{\text{II}}}$ is active to use only electrical motors when muscle is fatigued and needs recovery. Whether a muscle is fatigued or non-fatigued is determined by comparing the estimated fatigue state with the user-selected threshold values, $\overline{\mu}$ and $\underline{\mu}$. $\underline{\mu}$ is the lower threshold and $\hat{\mu} < \underline{\mu}$ is considered fatigued. $\overline{\mu}$ is the upper threshold and $\hat{\mu} > \overline{\mu}$ means that muscle recovers to a non-fatigued status. Note that it is always required to make $\overline{\mu} > \underline{\mu}$ to avoid the Zeno behavior [51] in a switch system.

The stability of the feedback control law in (3),(4),and (5)is proven by a Lyapunov stability analysis in [25]. The consequent closed-loop control system is able to drive the 1-DOF hybrid knee exoskeleton to generate a desired knee movements (knee extension and flexion), which is a pre-defined time-dependent trajectory, $q_d(t)$, of the knee joint angle. During the experiments in real time, the entire integrated system is described by the block diagram in Fig. 2.

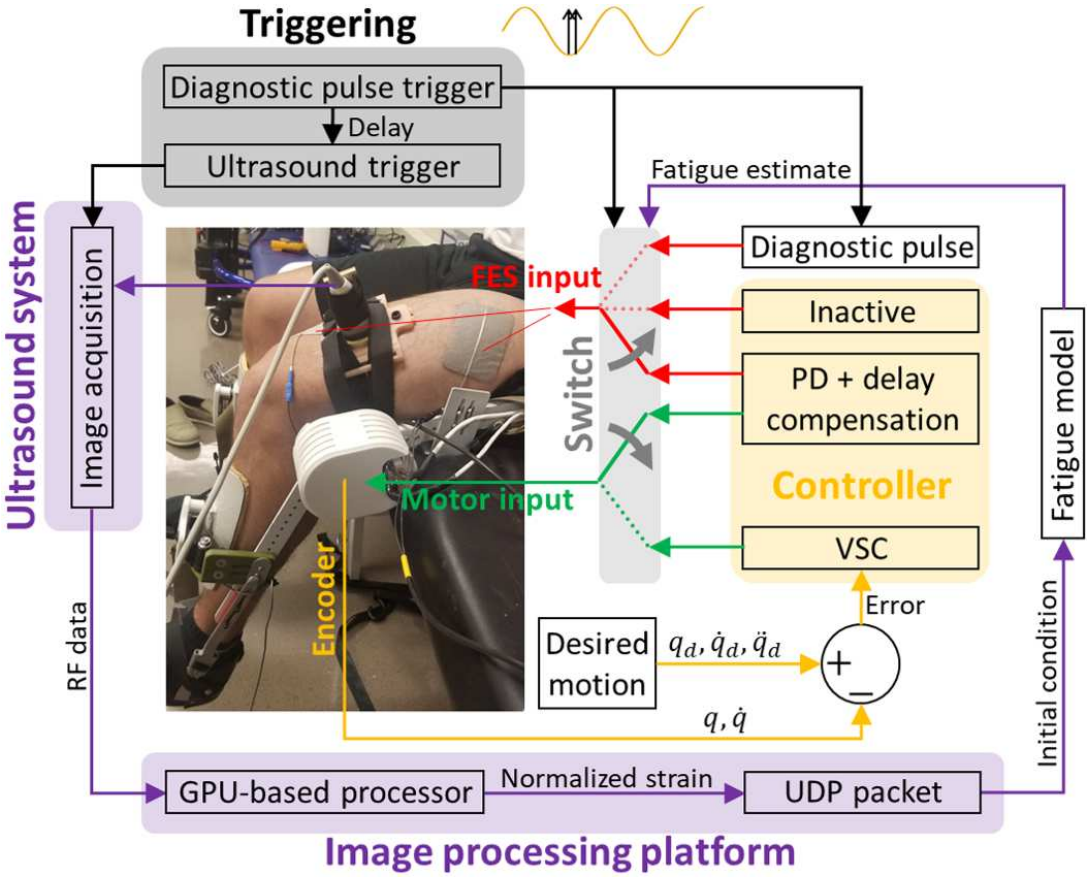

Figure 2. The block diagram that illustrates the design of the entire closed-loop system when feedback control and real-time ultrasound imaging are integrated. See the text for a detailed description. Radio frequency (RF) data refers to the raw ultrasound data before beamforming. VSC represents the variable structure control. UDP refers to the user datagram protocol used for data communication among the ultrasound imaging system, the image processing platform and the feedback controller.

C. Muscle Fatigue Estimation

Muscle fatigue in this study refers to the force generating efficiency that is a ratio of force produced by the current muscle contraction with respect to its maximum capability. Therefore, in (2), muscle fatigue is modeled by a time variant multiplier, $\hat{\mu}$, which modulates the control inputs contributed from FES-stimulated muscle contractions. The estimate of the FES-induced muscle fatigue, $\hat{\mu}$, combines the muscle contractility assessment from real-time processed ultrasound strain images and a modified first order predictive fatigue model [52], as

$$\begin{aligned}\dot{\hat{\mu}}^{(j)} &= \hat{w}_f^{(j)}(\varsigma^{(j)} - \hat{\mu}^{(j)})K_a^{(j)}u_{s,\tau^{(j)}}^{(j)} \\ &\quad + \hat{w}_r^{(j)}(1-\hat{\mu}^{(j)})(1-K_a^{(j)}u_{s,\tau^{(j)}}^{(j)}),\end{aligned} \tag{7}$$

where, $\hat{w}_f^{(j)} \in \mathbb{R}_{>0}$ and $\hat{w}_r^{(j)} \in \mathbb{R}_{>0}$ with the superscript $j = 1, 2$, are the estimated reciprocal of the fatigue constant and the recovery time constant, respectively. The parameters, $\hat{w}_f^{(j)}$ and $\hat{w}_r^{(j)}$ can be calculated by using a system identification procedure [12]. Note that, for any finite time interval, the evolution of $\hat{\mu}$ according to (7) relies on a known initial condition. Therefore, the role of the ultrasound imaging is to re-initialize the predictive fatigue model, (7), by providing the most updated initial condition when a new ultrasound measurement sample is available. The ultrasound imaging estimates muscle's strain tensor, which reflects the muscle deformation during contraction. According to the results in our previous studies [43], [44], there exists a potential correlation between the strain measure and the force produced by muscle contraction. Considering the aforementioned definition of $\hat{\mu}$ that is the the force generating efficiency, we can then estimate the percentage drop of $\hat{\mu}$ from the initial value of 1 by the percentage drop of the strain value. Considering the online computation speed with the current parameters used for real-time ultrasound image processing, the ultrasound imaging measurements are available every 20 seconds during the experiments.

D. Real-Time Ultrasound Strain Imaging Implementation

1) Diagnostic Imaging Procedure: To imitate the methodology of ultrasound imaging-based muscle fatigue assessment (as in [43], [44]) in the real-time control system, a "diagnosis-imaging" procedure is designed. Specifically, as illustrated by the sketch at the top of Fig. 2, when the desired motion trajectory, $q_d(t)$ (chosen as a sinusoidal curve in the current experiment), periodically reaches its minimum, two consecutive short pulses as trigger signals are generated accurately at that time instance. The first pulse is used to interrupt the controller-calculated error-modulated FES input and replace it

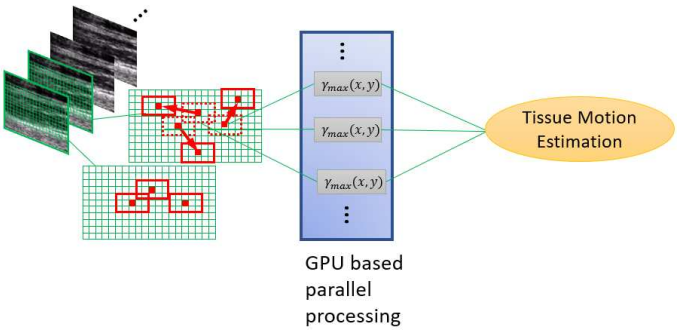

Figure 3. Workflow for parallel computation of the 2-D cross-correlation used for real-time implementation. It is noted that the cross-correlation computation at each point in the region of interest in (8) is independent. The ultrasound images are loaded onto the GPU and the cross-correlation, $\gamma(x, y)$, is computed simultaneously at every point in the region of interest.

with a constant 1-second "diagnostic" FES input. The second pulse is delayed for $100 \sim 300$ ms after the first pulse. It is used to trigger a short time window when the ultrasound image acquisition and processing are active to assess the muscle's response to the "diagnostic" FES input. The reason for locating the trigger signals at the valley of a sinusoidal is that, around that time, the actual knee movement under the feedback control also reaches the valley, i.e., velocity is zero and the quadriceps muscle is at a relaxed status. Then the applied "diagnosis-imaging" procedure is similar to the isometric knee extension experiment, as reported in [43], [44].

A triggering delay in the second pulse for ultrasound imaging considers the EMD in muscle's response after the diagnostic FES. Thus, we can efficiently allocate the hardware and computation resources and focus in a time window when a dominant muscle contraction occurs. Due to the current limitation of computation speed in ultrasound image processing, the designed "diagnosis-imaging" procedure is repeated, and ultrasound image measurements are available every 20 seconds.

When ultrasound image measurements are obtained, the raw radio frequency (RF) data is passed to the GPU-based image processing platform. The images are reconstructed by a delay-and-sum (DAS) beamformer and the ultrasound speckle tracking is performed to calculate muscle's displacement field. Strain images are then calculated based on the gradient of the displacement field. Due to the force-strain correlation discussed in [43], [44], the average of the strain image is calculated and normalized to approximate the fatigue state, $\hat{\mu}$, at the current time instant. This value is then passed to the predictive fatigue model, (7), and used as the new initial condition of the fatigue model during the time period when ultrasound image measurements are not available. Then the estimate of the fatigue state during this period (between two consecutive available ultrasound image measurements) is calculated by the re-initialized fatigue model. Finally, the fatigue estimate is passed to the feedback controller to determine the switches between control mode $u_{m_{\mathrm{I}}}$ and $u_{m_{\mathrm{II}}}$.

2) GPU-Based Ultrasound Imaging Processing: The original speckle tracking algorithm used for tissue motion estimation in [43], [44] is based on exhaustively searching the displacement vector candidate (from the reference frame to the moving frame) that makes the normalized cross-correlation coefficient the maximum. It has a good performance to estimate tissue motion to the level of about 0.01 mm. However, it is difficult to satisfy real-time capabilities required for closed-loop control. This is due to that the computation cost increases quadratically with the size of the kernel and search window in the following 2D normalized cross-correlation computation,

$$\gamma(x,y) = \frac{\sum_{K_{x,y}}(f_m(a,b)-\bar{f}_m)(f_n(a+u,b+v)-\bar{f}_{n,u,v})}{\sqrt{\sum_{K_{x,y}}(f_m(a,b)-\bar{f}_m)^2(f_n(a+u,b+v)-\bar{f}_{n,u,v})^2}}, \tag{8}$$

where, γ is the normalized correlation coefficient at location, (x, y), f_m and f_n refer to magnitude of the ultrasound image signal from frame number m and n, respectively. $(a, b) \in K_{x,y}$. $K_{x,y}$ is the rectangular kernel centered at position (x, y). Inside the kernel, signal magnitude at all the locations are used to compute the similarity measure that is the normalized cross-correlation, γ. For computing γ, $\bar{f}_m$, $\bar{f}_{n,u,v}$ are mean values of $f_m(a, b)$ and $f_n(a + u, b + v)$, respectively. $u(x, y)$ and $v(x, y)$ are the offsets that form the displacement vector, (u, v) at location (x, y).

According to the form of $\gamma(x, y)$ that can be computed independently at different locations, (x, y), the speckle tracking algorithm can be implemented using a GPU architecture that enables parallel computing to accelerate the overall computation to achieve real-time strain measurements. By further tuning the speckle tracking parameters, such as the size of the region of interest and kernel, to balance the image processing quality and the real-time requirement, the processing time to compute the strain between two consecutive images was eventually reduced to < 1 second when implemented on the GPU. The workflow for the parallel computing implementation is shown in Fig. 3.

III. Experiments

The objective of the experiments in this study is to demonstrate the feasibility of using real-time ultrasound imaging to estimate muscle fatigue, which assists the decision-making of control mode switches in the closed-loop feedback control system. The Institutional Review Board of North Carolina State University approved all the procedures and protocols of the experiments. A male human participant with no disabilities consented to participate in the experiments. Seven trials were performed. As shown in Fig. 1, during each trial, the participant wore the hybrid knee exoskeleton and the feedback controller controls his knee joint to follow a pre-defined 200-second sinusoidal trajectory, $q_d(t) = 20\sin(\pi t/5)$. The initial offset angle, q_0, as illustrated in Fig. 1, is chosen to be approximately $45°$. The control mode of the feedback controller switches between a PD-based delay compensation controller (FES and motor) and a VSC controller (motor only) according to the switch criteria. The upper ($\overline{\mu}$) and lower ($\underline{\mu}$) threshold of the fatigue-based switch is set as 0.9 and 0.8, respectively.

The knee joint is actuated by the torque produced by stimulated contractions of a quadriceps-hamstring muscle pair,

as well as by an electric motor (Harmonic Drive LLC, MA, USA). The stimulation is achieved using a commercial stimulator (Rehastim 2, HASOMED GmbH, Germany) which administered biphasic FES at a frequency of 33 Hz and a pulse width 300 μs through electrode pads (PALS, 7.62 cm by 10.16 cm, Axelgaard Manufacturing Co., Ltd., USA) placed on both the quadriceps and hamstrings. The knee joint angle is measured by the internal relative encoders of the electric motors. The entire closed-loop system, as illustrated in Fig. 2, is implemented and programmed in a real-time XPC target (Speedgoat GmbH, Switzerland) using MATLAB/Simulink (MathWorks, USA).

A clinical ultrasound linear transducer (L7.5SC Prodigy Probe, S-Sharp, Taiwan) was placed longitudinally on the thigh. It was fixed by a customized probe holder to image the targeted quadriceps muscle. The ultrasound planewave imaging, with a center frequency of 5 MHz and a sampling frequency of 20 MHz, was implemented in the ultrasound imaging system (Prodigy Research Platform, S-Sharp, Taiwan). Considering the trade-off between the computation speed and the performance of the speckle tracking algorithm, we tested different frame rates (250, 500, 800, 1000, 1600 Hz) of ultrasound imaging in different experiment trials. The image processing platform uses a GPU (Titan V, NVIDIA, USA). Data exchange among the XPC target, the ultrasound imaging system, and the image processing platform is achieved through a user datagram protocol (UDP). The control gains along with fatigue parameters and FES saturation and threshold are shown in Table I.

IV. Results and Discussion

Seven trials were performed to test the integration of real-time ultrasound imaging into the closed-loop control system of the 1-DOF hybrid knee exoskeleton. Table II summarizes the experiment results while Fig. 4 is the graphic presentation of trial 4. The RMSE is calculated between the encoder registered knee joint angle (q, solid orange curve in the first row of Fig. 4) and the desired knee joint angle (q_d, dotted blue curve in the first row of Fig. 4). The results show a good control performance (error less than 2°) under the designed closed-loop control system despite the occurrence of the fatigue-based switches between different control modes, as well as the "diagnostic" FES input (that acts as a disturbance from the controller's point of view). The switching behavior is also successfully achieved according to the designed fatigue-based switch criteria when the assessing FES-induced muscle fatigue is based on real-time ultrasound imaging. The shadowed region in Fig. 4 denotes the switch to the VSC controller (motor only) when the estimated fatigue state is below the chosen lower threshold (0.8). The second row of Fig. 4 plots the time-variant value of the FES input to the quadriceps muscle by the solid red curve. The baseline of this curve (21 mA) reflects the threshold level of the participant's muscle, above which the FES input can generate a noticeable muscle response (i.e., a noticeable force generation during preliminary isometric muscle contraction experiments). The periodically occurring squared pulses with a high peak (30 mA) reflect the "diagnostic" FES input. In contrast, the flat part (approximately between 60 s and 80 s) reflects the deactivation of FES when the muscle is considered as "fatigued" (below the lower threshold, 0.8) and the alternative control mode (VSC, motor only) is used. The FES input to the hamstring muscle is omitted because its value is minimal (in the order of 10^{-1} mA above the baseline).

In addition, as is observed from the last row of Fig. 4, the jumps on the model-based fatigue curve (solid black curve) reflect the re-initialization of the predictive model when a most updated measurement from real-time ultrasound imaging (purple circle) is acquired. The first ultrasound measurement is used as the baseline for strain normalization and is not used to re-initialize the model. A small jump on the fatigue curve indicates a relatively good agreement between the ultrasound-assessed and the model-predicted fatigue state. In contrast, a significant jump shows a considerable discrepancy between the ultrasound measurement and the model prediction at the specific time instance. However, at the current stage of our study, it is difficult to determine which one is closer to the absolute ground truth because multiple uncertainties exist in both processes for identifying the fatigue model and the strain-force correlation. In fact, for the predictive fatigue model, due to its dependency on accurate model parameters and the initial condition, the bias of fatigue estimation is expected to accumulate over time. Thus, the model needs re-initialization by the real-time ultrasound measurements. However, the obtained ultrasound measurements themselves have a noisy aspect and can sometimes have inconsistent oscillations between samples on the time horizon. This is because the ultrasound measurements are separate independent data samples and do not constrain the temporal trend. This potentially brings significant variance to and affects the fatigue estimation when these samples are repeatedly used to re-initialize the model, especially when the sampling rate of the ultrasound assessment is low (every 20 s) due to the limitation of computation speed. One potential solution is to optimize the image processing platform further to increase the computation speed to obtain ultrasound measurements more frequently. In this way, when more consecutive data samples are available during a specific time window, filtering techniques can be applied to mitigate the noisy aspect of the signals. An alternative solution is to combine the predictive fatigue model and intermittently available ultrasound measurements in an observer-like structure. In this way, due to the ultrasound measurements, the predictive fatigue model no longer relies on an accurately known initial condition, while the temporal theoretical trend provided by the model can be used as a temporal constraint to regularize the ultrasound measurements.

V. Conclusion

For the first time, this paper designs and implements a closed-loop control system of a one-DOF hybrid knee exoskeleton that integrates real-time ultrasound imaging for FES-induced muscle fatigue assessment. The experiment results show the feasibility of applying ultrasound imaging for tissue strain estimation as an indicator of muscle fatigue and

Table I
LIST OF PARAMETERS USED IN EXPERIMENT

Parameter	α	β	K_u	K_v	r_c	w_f (s^{-1})	w_r (s^{-1})	**sat (mA)**	**thresh (mA)**
Value	80	2	2	2	0.05	1/11	1/25	50	21

Table II
RESULTS OF KNEE JOINT TRACKING USING THE DESIGNED CLOSED-LOOP CONTROL SYSTEM.

Trial number		**1**	**2**	**3**	**4**	**5**	**6**	**7**
RMSE (°)		1.60	1.84	1.48	1.85	1.75	1.98	1.89
Switch threshold	**upper**	0.9	0.9	0.9	0.9	0.9	0.9	0.9
	lower	0.8	0.8	0.8	0.8	0.8	0.8	0.8
Ultrasound frame rate (Hz)		1600	250	500	500	1000	1000	800
Ultrasound trigger delay (ms)		100	100	100	160	160	160	160

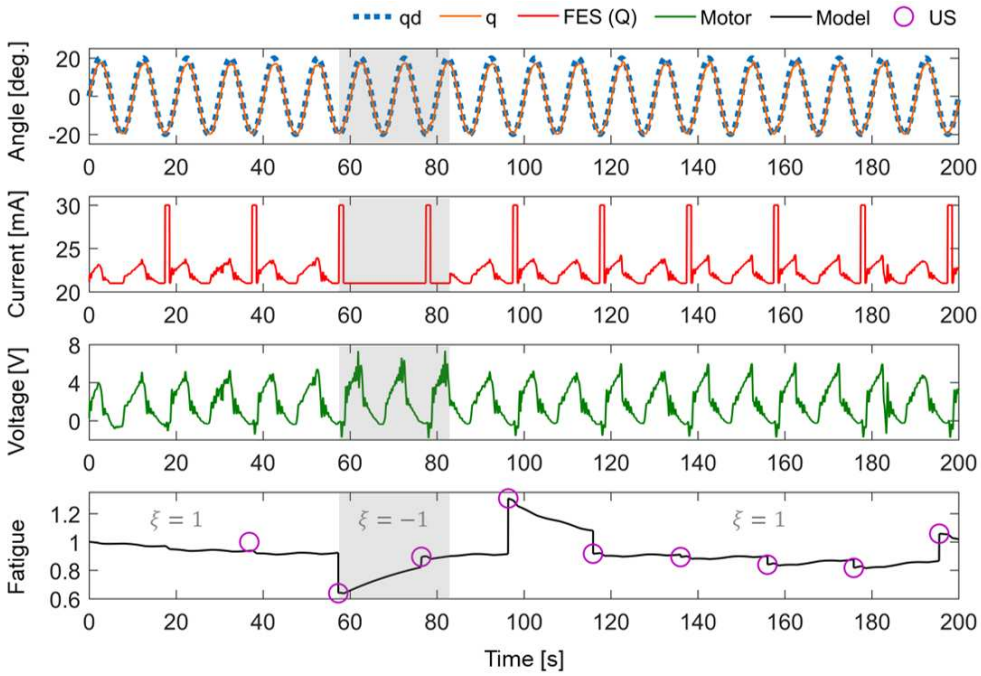

Figure 4. Graphical presentation of the experiment trial 4. The first row presents the actual knee joint angle (solid orange curve) to track the desired sinusoidal trajectory (dotted blue line). The second row presents the recorded FES input to the quadriceps muscle. The third row presents the recorded voltage input to the electrical motor. The last row presents the fatigue estimation obtained by using the obtained ultrasound (US) measurements to re-initialize the predictive fatigue model. The shadowed region indicates the switch to the VSC controller (motor only) when muscle is considered fatigued and FES is inactive.

subsequently facilitating the control system's switch behavior. The results show that FES and powered assistance can be switched between different assistive modes when the muscle undergoes a fatigue and recovery cycle while achieving a good control performance. This study shows that ultrasound imaging as a sensing modality in assistive devices helps feedback controllers in decision-making and potentially enables unrestrained, robust fatigue-resistant limb movements for functional tasks.

REFERENCES

[1] J. Chae, L. Sheffler, and J. Knutson, "Neuromuscular electrical stimulation for motor restoration in hemiplegia," *Top. Stroke Rehabil.*, vol. 15, no. 5, pp. 412–426, 2008.

[2] E. Marsolais and R. Kobetic, "Functional electrical stimulation for walking in paraplegia." *J. Bone Joint Surg.*, vol. 69, no. 5, pp. 728–733, 1987.

[3] P. H. Peckham and J. S. Knutson, "Functional electrical stimulation for neuromuscular applications," *Annu. Rev. Biomed. Eng.*, vol. 7, pp. 327–360, 2005.

[4] J. J. Abbas and H. J. Chizeck, "Feedback control of coronal plane hip angle in paraplegic subjects using functional neuromuscular stimulation," *IEEE Trans. Biomed. Eng.*, vol. 38, no. 7, pp. 687–698, 1991.

[5] C. L. Lynch and M. R. Popovic, "Functional electrical stimulation," *IEEE Control Syst. Mag.*, vol. 28, no. 2, pp. 40–50, 2008.

[6] C. Freeman, A.-M. Hughes, J. Burridge, P. Chappell, P. Lewin, and E. Rogers, "Iterative learning control of FES applied to the upper extremity for rehabilitation," *Control Eng. Pract.*, vol. 17, no. 3, pp. 368–381, 2009.

[7] A. Ajoudani and A. Erfanian, "A neuro-sliding-mode control with adaptive modeling of uncertainty for control of movement in paralyzed limbs using functional electrical stimulation," *IEEE Trans. Biomed. Eng.*, vol. 56, no. 7, pp. 1771–1780, 2009.

[8] N. Sharma, K. Stegath, C. M. Gregory, and W. E. Dixon, "Nonlinear neuromuscular electrical stimulation tracking control of a human limb," *IEEE Trans. Neural Syst. Rehabil. Eng.*, vol. 17, no. 6, pp. 576–584, 2009.

[9] E. Schearer, Y.-W. Liao, E. Perreault, M. Tresch, W. Memberg, R. Kirsch, and K. Lynch, "Multi-muscle FES force control of the human

arm for arbitrary goals," *IEEE Trans. Neural Syst. Rehabil. Eng.*, vol. 22, no. 3, pp. 654–663, 2014.
[10] S. N. Kukke and R. J. Triolo, "The effects of trunk stimulation on bimanual seated workspace," *IEEE Trans. Neural Syst. Rehabil. Eng.*, vol. 12, no. 2, pp. 177–185, 2004.
[11] N. Alibeji, N. Kirsch, and N. Sharma, "An adaptive low-dimensional control to compensate for actuator redundancy and FES-induced muscle fatigue in a hybrid neuroprosthesis," *Control Eng. Pract.*, vol. 59, pp. 204–219, 2017.
[12] N. A. Kirsch, X. Bao, N. A. Alibeji, B. E. Dicianno, and N. Sharma, "Model-based dynamic control allocation in a hybrid neuroprosthesis," *IEEE Trans. Neural Syst. Rehabil. Eng.*, vol. 26, no. 1, pp. 224–232, 2018.
[13] K. H. Ha, S. A. Murray, and M. Goldfarb, "An approach for the cooperative control of FES with a powered exoskeleton during level walking for persons with paraplegia," *IEEE Trans. Neural Syst. Rehabil. Eng.*, vol. 24, no. 4, pp. 455–466, 2016.
[14] C.-H. Chang, J. A. Casas, S. Brose, and V. H. Duenas, "Closed-loop torque and kinematic control of a hybrid lower-limb exoskeleton for treadmill stepping," *Front. Robot. AI*, vol. 8.
[15] X. Bao, Z. Sheng, B. E. Dicianno, and N. Sharma, "A tube-based model predictive control method to regulate a knee joint with functional electrical stimulation and electric motor assist," *IEEE Trans. Control Syst. Technol.*, vol. 25, no. 6, pp. 2180–2191, 2020.
[16] X. Bao, V. Molazadeh, A. Dodson, B. E. Dicianno, and N. Sharma, "Using person-specific muscle fatigue characteristics to optimally allocate control in a hybrid exoskeletonpreliminary results," *IEEE Trans. Med. Robot. Bionics*, vol. 2, no. 2, pp. 226–235, 2020.
[17] V. Molazadeh, Q. Zhang, X. Bao, B. E. Dicianno, and N. Sharma, "Shared control of a powered exoskeleton and functional electrical stimulation using iterative learning," *Front. Robot. AI*, vol. 8, 2021.
[18] A. J. Del-Ama, Á. Gil-Agudo, J. L. Pons, and J. C. Moreno, "Hybrid FES-robot cooperative control of ambulatory gait rehabilitation exoskeleton," *J. Neuroeng. Rehabil.*, vol. 11, no. 1, pp. 1–15, 2014.
[19] I. Jammeli, A. Chemori, H. Moon, S. Elloumi, and S. Mohammed, "An assistive explicit model predictive control framework for a knee rehabilitation exoskeleton," *IEEE/ASME Trans. Mechatronics*, 2021.
[20] M. K. Shepherd and E. J. Rouse, "Design and validation of a torque-controllable knee exoskeleton for sit-to-stand assistance," *IEEE/ASME Trans. Mechatronics*, vol. 22, no. 4, pp. 1695–1704, 2017.
[21] D. Currier and R. Mann, "Muscular strength development by electrical stimulation in healthy individuals," *Phys. Ther.*, vol. 63, no. 6, pp. 915–921, 1983.
[22] L. Griffin, M. Decker, J. Hwang, B. Wang, K. Kitchen, Z. Ding, and J. Ivy, "Functional electrical stimulation cycling improves body composition, metabolic and neural factors in persons with spinal cord injury," *J. Electromyogr. Kinesiol.*, vol. 19, no. 4, pp. 614–622, 2009.
[23] B. J. Andrews and G. D. Wheeler, "Functional and therapeutic benefits of electrical stimulation after spinal injury." *Curr. Opin. Neurol.*, vol. 8, no. 6, pp. 461–466, 1995.
[24] C. S. Bickel, C. M. Gregory, and J. C. Dean, "Motor unit recruitment during neuromuscular electrical stimulation: a critical appraisal," *Eur. J. Appl. Physiol.*, vol. 111, no. 10, pp. 2399–2407, 2011.
[25] Z. Sheng, Z. Sun, V. Molazadeh, and N. Sharma, "Switched control of an n-degree-of-freedom input delayed wearable robotic system," *Automatica*, vol. 125, p. 109455, 2021.
[26] J. Ding, A. Wexler, and S. Binder-Macleod, "A predictive fatigue model. I. predicting the effect of stimulation frequency and pattern on fatigue," *IEEE Trans. Rehabil. Eng.*, vol. 10, no. 1, pp. 48–58, 2002.
[27] L. A. Frey-Law, J. M. Looft, and J. Heitsman, "A three-compartment muscle fatigue model accurately predicts joint-specific maximum endurance times for sustained isometric tasks," *J. Biomech.*, vol. 45, no. 10, pp. 1803–1808, 2012.
[28] J. Z. Liu, R. W. Brown, and G. H. Yue, "A dynamical model of muscle activation, fatigue, and recovery," *Biophys. J.*, vol. 82, no. 5, pp. 2344–2359, 2002.
[29] R. Riener, J. Quintern, and G. Schmidt, "Biomechanical model of the human knee evaluated by neuromuscular stimulation," *J. Biomech.*, vol. 29, pp. 1157–1167, 1996.
[30] J. Ding, A. Wexler, and S. Binder-Macleod, "A predictive fatigue model. II. predicting the effect of resting times on fatigue," *IEEE Trans. Rehabil. Eng.*, vol. 10, no. 1, pp. 59–67, 2002.
[31] J. Heckmatt, N. Pier, and V. Dubowitz, "Real-time ultrasound imaging of muscles," *Muscle Nerve*, vol. 11, no. 1, pp. 56–65, 1988.
[32] D. J. Critchley and F. J. Coutts, "Abdominal muscle function in chronic low back pain patients: measurement with real-time ultrasound scanning," *Physiotherapy*, vol. 88, no. 6, pp. 322–332, 2002.
[33] K. Van, J. A. Hides, and C. A. Richardson, "The use of real-time ultrasound imaging for biofeedback of lumbar multifidus muscle contraction in healthy subjects," *J. Orthop. Sports Phys. Ther.*, vol. 36, no. 12, pp. 920–925, 2006.
[34] M. Shinohara, K. Sabra, J.-L. Gennisson, M. Fink, and M. Tanter, "Real-time visualization of muscle stiffness distribution with ultrasound shear wave imaging during muscle contraction," *Muscle Nerve*, vol. 42, no. 3, pp. 438–441, 2010.
[35] J. A. Hides, C. A. Richardson, and G. A. Jull, "Use of real-time ultrasound imaging for feedback in rehabilitation," *Man. Ther.*, vol. 3, no. 3, pp. 125–131, 1998.
[36] S. Kuno and T. Fukunaga, "Measurement of muscle fibre displacement during contraction by real-time ultrasonography in humans," *Eur. J. Appl. Physiol. Occup. Physiol.*, vol. 70, no. 1, pp. 45–48, 1995.
[37] P. Hodges, L. Pengel, R. Herbert, and S. Gandevia, "Measurement of muscle contraction with ultrasound imaging," *Muscle Nerve*, vol. 27, no. 6, pp. 682–692, 2003.
[38] Q. Zhang, K. Kim, and N. Sharma, "Prediction of ankle dorsiflexion moment by combined ultrasound sonography and electromyography," *IEEE Trans. Neural. Syst. Rehabil. Eng.*, vol. 28, no. 1, pp. 318–327, 2019.
[39] Q. Zhang, A. Iyer, K. Kim, and N. Sharma, "Evaluation of non-invasive ankle joint effort prediction methods for use in neurorehabilitation using electromyography and ultrasound imaging," *IEEE Trans. Biomed. Eng.*, vol. 68, no. 3, pp. 1044–1055, 2020.
[40] C. Castellini, G. Passig, and E. Zarka, "Using ultrasound images of the forearm to predict finger positions," *IEEE Trans. Neural Syst. Rehabil. Eng.*, vol. 20, no. 6, pp. 788–797, 2012.
[41] D. Sierra González and C. Castellini, "A realistic implementation of ultrasound imaging as a human-machine interface for upper-limb amputees," *Front. Neurorobot.*, vol. 7, pp. 17:1–17:11, 2013.
[42] S. Sikdar, H. Rangwala, E. B. Eastlake, I. A. Hunt, A. J. Nelson, J. Devanathan, A. Shin, and J. J. Pancrazio, "Novel method for predicting dexterous individual finger movements by imaging muscle activity using a wearable ultrasonic system," *IEEE Trans. Neural Syst. Rehabil. Eng.*, vol. 22, no. 1, pp. 69–76, 2014.
[43] Z. Sheng, N. Sharma, and K. Kim, "Quantitative assessment of changes in muscle contractility due to fatigue during nmes: An ultrasound imaging approach," *IEEE Trans. Biomed. Eng.*, vol. 67, no. 3, pp. 832–841, 2019.
[44] ——, "Ultra-high-frame-rate ultrasound monitoring of muscle contractility changes due to neuromuscular electrical stimulation." *Ann. Biomed. Eng.*, 2020.
[45] M. A. Lubinski, S. Y. Emelianov, and M. O'Donnell, "Speckle tracking methods for ultrasonic elasticity imaging using short-time correlation," *IEEE Trans. Ultrason. Ferroelectr. Freq. Control*, vol. 46, no. 1, pp. 82–96, 1999.
[46] J. Y. Liu, J. Xu, F. Forsberg, J.-B. Liu *et al.*, "Cmut/cmos-based butterfly iq-a portable personal sonoscope," *Advanced Ultrasound in Diagnosis and Therapy*, vol. 3, no. 3, pp. 115–118, 2019.
[47] N. Akhlaghi, A. Dhawan, A. A. Khan, B. Mukherjee, G. Diao, C. Truong, and S. Sikdar, "Sparsity analysis of a sonomyographic muscle–computer interface," *IEEE Trans. Biomed. Eng.*, vol. 67, no. 3, pp. 688–696, 2019.
[48] X. Yang, J. Yan, Y. Fang, D. Zhou, and H. Liu, "Simultaneous prediction of wrist/hand motion via wearable ultrasound sensing," *IEEE Trans. Neural Syst. Rehabil. Eng.*, vol. 28, no. 4, pp. 970–977, 2020.
[49] B. Peng, Y. Wang, T. J. Hall, and J. Jiang, "A gpu-accelerated 3-d coupled subsample estimation algorithm for volumetric breast strain elastography," *IEEE Trans. Ultrason. Ferroelectr. Freq. Control*, vol. 64, no. 4, pp. 694–705, 2017.
[50] T. Idzenga, E. Gaburov, W. Vermin, J. Menssen, and C. L. De Korte, "Fast 2-d ultrasound strain imaging: The benefits of using a gpu," *IEEE Trans. Ultrason. Ferroelectr. Freq. Control*, vol. 61, no. 1, pp. 207–213, 2014.
[51] R. Goebel, R. G. Sanfelice, and A. R. Teel, "Hybrid dynamical systems," *IEEE Control Syst. Mag.*, vol. 29, no. 2, pp. 28–93, 2009.
[52] N. Sharma, N. A. Kirsch, N. A. Alibeji, and W. E. Dixon, "A non-linear control method to compensate for muscle fatigue during neuromuscular electrical stimulation," *Front. Robot. AI*, vol. 4, 2017.